Parallel propagation and damping of electromagnetic waves in a partially ionized plasma with multiple species

Yifan Huang, Jiannan Tu, and Paul Song

Citation: Physics of Plasmas 25, 122101 (2018); doi: 10.1063/1.5053119

View online: https://doi.org/10.1063/1.5053119

View Table of Contents: http://aip.scitation.org/toc/php/25/12

Published by the American Institute of Physics

Articles you may be interested in

lon acoustic super solitary waves in a magnetized plasma Physics of Plasmas **25**, 122302 (2018); 10.1063/1.5063955

Inertial Alfvén solitons in quantum plasma with correction of temperature degeneracy

Physics of Plasmas 25, 124501 (2018); 10.1063/1.5055794

Plasma mass separation

Physics of Plasmas 25, 090901 (2018); 10.1063/1.5042845

Magnetosonic/whistler mode turbulence influences on ion dynamics

Physics of Plasmas 25, 122301 (2018); 10.1063/1.5053760

Effects of wave potential on electron holes in thermal and superthermal space plasmas

Physics of Plasmas 25, 122901 (2018); 10.1063/1.5046721

Analysis and comparison of ion-acoustic wave reflection using laser-induced fluorescence and Langmuir probes

Physics of Plasmas 25, 122102 (2018); 10.1063/1.5058805



Parallel propagation and damping of electromagnetic waves in a partially ionized plasma with multiple species

Yifan Huang, a) Jiannan Tu, and Paul Song
Space Science Lab, University of Massachusetts Lowell, Lowell, Massachusetts 01854.USA

(Received 21 August 2018; accepted 13 November 2018; published online 6 December 2018)

We study the propagation of electromagnetic waves (or incompressible waves with negligible thermal pressure) along the magnetic field in a partially ionized plasma with multiple species. Because of differences in mass and density, each species responds to and hence affects the perturbations of electromagnetic fields differently. Collisions among all the species further complicate the process. With a linear analysis, the dispersion relation of parallel propagation covering a large range of frequencies, from magnetohydrodynamics (MHD) waves to light waves, with an arbitrary combination of multiple positively charged species, negatively charged species, and neutral species is derived based on a multi-fluid treatment, in combination with Faraday's law and Ampere's law including the displacement current. In a collisional plasma, when the collision frequency is lower than the gyrofrequencies of charged species, the resonances are at the gyrofrequencies of each charged species and the cutoff frequencies are related to the densities of the charged species. Stopbands in which waves propagate with extremely high phase velocity but are strongly damped form between some of these characteristic frequencies. In the MHD wave frequency range, the coupling with neutral species slows the propagation speed compared with the Alfvén speed. The collisions between plasma and neutrons efficiently contribute to the wave damping, which is significantly reduced when the neutral species are completely driven with plasma by collisions. When the collisions become stronger, the resonances and cutoffs become weaker and may disappear. The species could couple tightly and act as a single fluid if the collisions among them are strong enough. Published by AIP Publishing. https://doi.org/10.1063/1.5053119

I. INTRODUCTION

Multiple ion species commonly exist in fusion and space plasmas, and charged dust grains can occur in laboratory and interstellar space. With multiple resonance and cutoffs of charged species, the dispersion behavior of the Alfvén waves is significantly affected, especially at frequencies close to the resonant and cutoff frequencies. In addition, the collisions between two different species may affect the coupling of species and the damping of the waves and thus affect the momentum and energy transport. Previous research studies have demonstrated the importance of the Alfvén waves in many fields, e.g., in the coupling between magnetosphere and ionosphere, $^{1-7}$ in solar corona heating, $^{8-10}$ and in laboratory 11 and fusion devices. 12 With multiple species and collisions among them, there may be some new or more precise effects beyond previous knowledge, e.g., strong damping of wave propagation due to collisions between ion species in interstellar clouds¹³ and interaction between solar wind with cometary plasma mainly determined by different ion species and grains. 14,15

In research of the magnetohydrodynamic (MHD) waves, a single-fluid treatment in MHD or Hall-MHD is widely used in many works, ^{16–19} but it neglects inertial terms of relative velocity between ion and neutral species in the momentum equation, and it is valid when the frequency of dynamics in the single-fluid treatment is much lower than the ionneutral collision frequency. A two-fluid treatment²⁰ where

ion-electron plasma and neutral species were treated as two separate fluids could have a larger range of applicability, but it still cannot tell the effects of the charged species even with electrons and ions. A three-fluid description⁴ of electrons, ions, and neutral species, including the inertia term of electrons, was developed to derive the dispersion relation for parallel propagating incompressible waves so that it could cover a larger frequency range, even to the resonant frequency of electrons. The derivation in the three-fluid treatment becomes so complicated that it has a barrier to include more ion species. Without considering the inertia term of electrons, a trial of five-fluid treatment²¹ could take into account the effects of three ion species studying parallel propagating incompressible waves.

On the other hand, the theory of wave propagation in a cold, fully ionized and collisionless plasma consisting of multiple species has been well developed by neglecting the pressure gradient of each species and employing a dielectric tensor to link the conducting current density and electric field. 22–28 It was shown that there are three principal plasma modes with left and right handed circularly polarized, and longitudinal perturbations, respectively. In a cold plasma, for parallel propagating waves, only Left-handed (L) and Right-handed (R) modes can propagate; for perpendicular propagating waves, only Extraordinary and Ordinary modes can propagate; for oblique propagating waves, only Fast and Slow modes, which are, respectively, described as the compressional Alfvén wave and the shear Alfvén wave in laboratory-oriented community, can propagate. With

a)Email: yifan_huang@student.uml.edu

multiple ion species, each ion species affects the propagation of the waves and may form its corresponding resonance and cutoff. Some studies presented experiments and simulations to observe and confirm the theoretical analysis about the wave propagation in multiple ion species. $^{30-33}$ The collision effects can be included in a multi-fluid model by simply assuming the collisional damping terms that are proportional to the velocity of the charged species and revising the mass terms, m_s , in momentum equations, 24,28 which is not suitable as the momentum exchange between two collision species is proportional to the relative velocity of them especially at low wave frequencies.

The present work is a new effort to present a more general fluid-approaching model to combine multiple species and collisions, and to study wave propagation in a multifluid plasma with an arbitrary number of species, including neutral species, by self-consistently considering all collisions among multiple species. Without neglecting the inertial motion of electrons, the model is thus applicable over very board frequency/time scale regimes, from low MHD wave frequencies to very high frequencies such as light waves. With an analytical dispersion relation of wave propagation, this model could be easily applied in a large parameter regime, from weakly ionized plasma in the low altitude ionosphere to highly ionized plasma in the magnetosphere, to study the propagation properties and damping. In Sec. II, we develop a multiple species treatment for parallel propagating waves and derive the general dispersion relation. In Sec. III, first we discuss a collisionless case to confirm the previous results under the same limits; second, we focus on a medium that includes electron, H^+ , O^+ , and neutral species and evaluate the dispersion relation with a range of density ratios, collision frequencies relative to the gyrofrequencies, and ionization fraction to discuss the resonances, cutoffs, phase velocity, and coupling of species. In Sec. IV, with simplifying approximations, we apply the knowledge gained to a magnetosphere-ionosphere-thermosphere system with an altitude range from 100 km to 1000 km to study the properties of the waves, based on empirical ionospheric and thermospheric models of the International Reference Ionosphere (IRI-2012)³⁴ and MSIS-E-90 Atmosphere, ³⁵ respectively.

II. GOVERNING EQUATIONS

We begin with the multiple fluid treatment to derive the wave dispersion relation. The governing equations can be obtained by integrating the Boltzmann equations over the phase space and defining the macroscopic quantities so that the individual particle motion is averaged out and the system is represented by macroscopic, or bulk, quantities such as bulk velocity, density, and pressure. The random collisions are represented by average collision frequencies. The momentum equations for each species as well as Faraday's Law and Ampere's Law are written as

$$\frac{\partial m_s n_s \vec{u}_s}{\partial t} + \nabla \cdot \left(\vec{P}_s + m_s n_s \vec{u}_s \vec{u}_s \right)
= n_s q_s (\vec{E} + \vec{u}_s \times \vec{B}) + \vec{F}_s + \frac{\delta \vec{M}_s}{\delta t}, \tag{1}$$

$$\nabla \times \vec{E} = -\frac{\partial \vec{B}}{\partial t},\tag{2}$$

$$\nabla \times \vec{B} = \mu_0 \vec{j} + \frac{1}{c^2} \frac{\partial \vec{E}}{\partial t}, \tag{3}$$

$$\vec{j} = \sum_{s} n_s q_s \vec{u}_s,\tag{4}$$

where \vec{u}_s , n_s , m_s , q_s , \vec{P}_s , \vec{j} , \vec{E} , \vec{B} , μ_0 , and c are the bulk velocity, number density, mass of a single particle, charge of a single particle, pressure tensor of species s, current density, electric field, magnetic field, permeability constant, and speed of light, respectively, \vec{F}_s is the external force on species s, and $\delta \vec{M}_s / \delta t$ is the collision term³⁶ which is defined as

$$\frac{\delta \vec{M}_s}{\delta t} = -\sum_t n_s m_s \nu_{st} (\vec{u}_s - \vec{u}_t), \tag{5}$$

where ν_{st} is the momentum transfer collision frequency, defined as

$$\nu_{st} = \frac{16}{3} \frac{n_t m_t}{m_s + m_t} \Phi_{st}^{(1,1)}.$$
 (6)

 $\Phi_{st}^{(L,I)}$ is the Chapman-Cowling collision integrals, and ν_{st} is defined when L=1, J=1. Physically, for any species s, a collision on average takes place every $\tau = 1/\sum_t \nu_{st}$. A particle of species s collides with a particle of species t every $\tau_{st} = 1/\nu_{st}$. Collisions are assumed to be elastic, e.g., no radiation is produced as a result of the collision. After each collision, the motions of the pair of colliding particles are assumed to be totally random. The reset of the particle motion is constrained by the momentum and energy conservation before and after the collision in the frame of reference of the center of mass of the two particles. Afterward the local electromagnetic and mechanical forces control the motion of each particle until the next collision for each of them. It is noted that the momentum transfer collision frequencies are not equal with respect to the two species but satisfy the following relation due to the conservation of momentum:

$$n_s m_s \nu_{st} = n_t m_t \nu_{ts}. \tag{7}$$

III. PARALLEL PROPAGATING ELECTROMAGNETIC WAVES

To derive the wave dispersion relation, we assume a monochromatic perturbation which propagates as a plane wave along the magnetic field that is assumed in the z-direction, and all species are initially at rest to a common frame of reference before the arrival of a wave perturbation. Then, the perturbation is proportional to $\exp[i(kz-\omega t)]$ and we neglect any terms that are of the second order or higher with respect to the perturbation quantities. In a cold plasma, the thermal pressure term of the momentum equations has no effects. Continuity and energy equations are not necessary for such a system. Then, the momentum equations for species s in this frame of reference can be reduced as

$$m_s n_s \frac{\partial \vec{u}_s}{\partial t} = n_s q_s (\vec{E} + \vec{u}_s \times \vec{B}_0) - \sum_t m_s n_s \nu_{st} (\vec{u}_s - \vec{u}_t), \quad (8)$$

which can also represent the neutral momentum equation when $q_s = 0$. To derive the dispersion relation from Eqs. (2)–(4) and (8), we use a matrix expression in which the species are indexed with numbers instead of names of the species for simplicity. Here, we just use four species to illustrate the derivation without losing the generality of an arbitrary number of species. Rewrite Eq. (8) in a matrix form

$$\partial_{t} \begin{pmatrix} \vec{u}_{1} \\ \vec{u}_{2} \\ \vec{u}_{3} \\ \vec{u}_{4} \end{pmatrix} = \begin{pmatrix} q_{1}/m_{1} \\ q_{2}/m_{2} \\ q_{3}/m_{3} \\ q_{4}/m_{4} \end{pmatrix} \vec{E} + \begin{pmatrix} q_{1}\vec{u}_{1}/m_{1} \\ q_{2}\vec{u}_{2}/m_{2} \\ q_{3}\vec{u}_{3}/m_{3} \\ q_{4}\vec{u}_{4}/m_{4} \end{pmatrix} \times \vec{B}_{0} + [\nu_{4\times4}] \begin{pmatrix} \vec{u}_{1} \\ \vec{u}_{2} \\ \vec{u}_{3} \\ \vec{u}_{4} \end{pmatrix},$$
(9)

where

$$[\nu_{4\times4}] = \begin{pmatrix} -(\nu_{12} + \nu_{13} + \nu_{14}) & \nu_{12} & \nu_{13} & \nu_{14} \\ \nu_{21} & -(\nu_{21} + \nu_{23} + \nu_{24}) & \nu_{23} & \nu_{24} \\ \nu_{31} & \nu_{32} & -(\nu_{31} + \nu_{32} + \nu_{34}) & \nu_{34} \\ \nu_{41} & \nu_{42} & \nu_{43} & -(\nu_{12} + \nu_{13} + \nu_{14}) \end{pmatrix}.$$
(10)

By plugging Eq. (3) into the curl of Eq. (2), we obtain a relationship that connects the current density and the electric field

$$\partial_t \vec{j} = -\frac{1}{\mu_0} \left(\vec{\nabla} \times \vec{\nabla} \times \vec{E} + \frac{1}{c^2} \partial_t^2 \vec{E} \right) = \frac{1}{\mu_0} \left(\vec{\nabla}^2 - \frac{1}{c^2} \partial_t^2 \right) \vec{E},$$
(11)

in which $\nabla \cdot \vec{E} = 0$ has been used because the electric field perturbation is in the x-y plane when the electromagnetic wave propagates along the magnetic field (z-axis). Even with collisions, the perturbations of velocities of each species are all in the plane perpendicular to the z axis. For electrostatic waves, although $\nabla \cdot \vec{E} \neq 0$, the wave does not propagate along the magnetic field and, hence, we do not consider the electrostatic waves in our current work. With

$$\vec{j} = (q_1 n_1 \quad q_2 n_2 \quad q_3 n_3 \quad q_4 n_4) \begin{pmatrix} \vec{u}_1 \\ \vec{u}_2 \\ \vec{u}_3 \\ \vec{u}_4 \end{pmatrix}, \tag{12}$$

we can eliminate \vec{E} by taking operator $\left(\vec{\nabla}^2 - \frac{1}{c^2}\partial_t^2\right)/\mu_0$ on both sides in Eq. (9) and rewrite it as

$$[C_1] \begin{pmatrix} \vec{u}_1 \\ \vec{u}_2 \\ \vec{u}_3 \\ \vec{u}_4 \end{pmatrix} + [C_2] \begin{pmatrix} \vec{u}_1 \\ \vec{u}_2 \\ \vec{u}_3 \\ \vec{u}_4 \end{pmatrix} \times \vec{B}_0 = 0, \tag{13}$$

where

$$[C_{1}] = \frac{1}{\mu_{0}} \left(\vec{\nabla}^{2} - \frac{1}{c^{2}} \partial_{t}^{2} \right) (-\partial_{t} + [\nu_{4 \times 4}]) + \begin{pmatrix} q_{1}/m_{1} \\ q_{2}/m_{2} \\ q_{3}/m_{3} \\ q_{4}/m_{4} \end{pmatrix} \left(q_{1}n_{1} \quad q_{2}n_{2} \quad q_{3}n_{3} \quad q_{4}n_{4} \right) \partial_{t},$$

$$(14)$$

$$[C_2] = \frac{1}{\mu_0} \left(\vec{\nabla}^2 - \frac{1}{c^2} \partial_t^2 \right) \begin{pmatrix} q_1/m_1 & 0 & 0 & 0\\ 0 & q_2/m_2 & 0 & 0\\ 0 & 0 & q_3/m_3 & 0\\ 0 & 0 & 0 & q_4/m_4 \end{pmatrix}.$$
(15)

For a parallel propagating incompressible wave, since the perturbations of species as well as the electric field are in the x-y plane, $\vec{u}_s \cdot \hat{B_0} = 0$ where $\hat{B_0}$ is the unit vector of the background field. With the fact $(\vec{u}_s \times \hat{B_0}) \times \hat{B_0} = -\vec{u}_s$, we can make a mathematical replacement $\times \hat{B_0} \to \Theta$, in which $\Theta^2 = -1$. Obviously $\Theta = \pm i$ physically corresponding to the R and the L modes, respectively, because the Lorenz force, which is related to $\times \hat{B_0}$, is the cause of the rotation of the motions and the circular polarization of the electric field. Therefore, Eq. (13) changes to (after making replacements of $\nabla \to i\vec{k}$, $\partial_t \to -i\omega$)

$$\omega \begin{pmatrix} if_{1} + X_{1} - \frac{\omega_{p1}^{2}}{K^{2}} & -if_{12} - \frac{\Omega_{1}\omega_{p2}^{2}}{\Omega_{2}K^{2}} & -if_{13} - \frac{\Omega_{1}\omega_{p3}^{2}}{\Omega_{3}K^{2}} & -if_{14} - \frac{\Omega_{1}\omega_{p4}^{2}}{\Omega_{4}K^{2}} \\ -if_{21} - \frac{\Omega_{2}\omega_{p1}^{2}}{\Omega_{1}K^{2}} & if_{2} + X_{2} - \frac{\omega_{p2}^{2}}{K^{2}} & -if_{23} - \frac{\Omega_{2}\omega_{p3}^{2}}{\Omega_{3}K^{2}} & -if_{24} - \frac{\Omega_{2}\omega_{p4}^{2}}{\Omega_{4}K^{2}} \\ -if_{31} - \frac{\Omega_{3}\omega_{p1}^{2}}{\Omega_{1}K^{2}} & -if_{32} - \frac{\Omega_{3}\omega_{p2}^{2}}{\Omega_{2}K^{2}} & if_{3} + X_{3} - \frac{\omega_{p3}^{2}}{K^{2}} & -if_{34} - \frac{\Omega_{3}\omega_{p4}^{2}}{\Omega_{4}K^{2}} \\ -if_{41} - \frac{\Omega_{4}\omega_{p1}^{2}}{\Omega_{1}K^{2}} & -if_{42} - \frac{\Omega_{4}\omega_{p2}^{2}}{\Omega_{2}K^{2}} & -if_{43} - \frac{\Omega_{4}\omega_{p3}^{2}}{\Omega_{3}K^{2}} & if_{4} + X_{4} - \frac{\omega_{p4}^{2}}{K^{2}} \end{pmatrix} = 0,$$

$$(16)$$

where $\Omega_s = q_s B_0/m_s$ and $\omega_{ps} = \sqrt{n_s q_s^2/(\varepsilon_0 m_s)}$ are the cyclotron frequency and plasma frequency, respectively, of species s, $v_s = \sum_{t \neq s} v_{st}$, $K^2 = -c^2 k^2 + \omega^2$, $X_s = 1 - i\Theta\Omega_s/\omega$, $f_{st} = \nu_{st}/\omega$. For convenience, the gyrofrequency of an ion is positive and the gyrofrequency of an anion is negative. Notice that Eq. (16) is in its general form including the neutral species of which the gyrofrequency and plasma frequency are both zero. The if_{st} terms depend on collisions and $\frac{\Omega_s \omega_{pt}^2}{\Omega_t K^2}$ is a factor due to the transformation from \vec{E} to the velocities, \vec{u}_s . To have a nontrivial solution, the determinant of the coefficient matrix must be zero, leading to an algebraic equation of the 8th order (2s order if there are s species) of frequency in the determinant. We are interested in the solutions of non-zero frequency. The general dispersion relation of wave propagation along the magnetic field in a medium with multiple species (see the Appendix) is

$$\frac{1}{c^{2}} - \frac{k^{2}}{\omega^{2}} = \frac{\mu_{0}}{B_{0}^{2}} \begin{pmatrix} \Omega_{1}/\omega \\ \vdots \\ \Omega_{p}/\omega \\ \vdots \\ \Omega_{s}/\omega \end{pmatrix}^{T} ([S] - i[\nu]^{T})^{-1}[\rho] \begin{pmatrix} \Omega_{1}/\omega \\ \vdots \\ \Omega_{p}/\omega \\ \vdots \\ \Omega_{s}/\omega \end{pmatrix},$$
(17)

where [S] is related to the gyrofrequencies of species and the polarization of waves, defined as

$$[S] = \begin{pmatrix} 1 \pm \Omega_1/\omega & & & & \\ & \ddots & & & \\ & & 1 \pm \Omega_p/\omega & & \\ & & & \ddots & \\ & & & 1 \pm \Omega_s/\omega \end{pmatrix}, (18)$$

 $[\nu]$ is the collision matrix

$$[\nu] = \begin{pmatrix} -\sum_{t \neq 1} \nu_{1t}/\omega & \cdots & \nu_{1p}/\omega & \dots & \nu_{1s}/\omega \\ \vdots & \ddots & \vdots & & \vdots \\ \nu_{p1}/\omega & \cdots & -\sum_{t \neq p} \nu_{pt}/\omega & \cdots & \nu_{ps}/\omega \\ \vdots & & \vdots & \ddots & \vdots \\ \nu_{s1}/\omega & \cdots & \nu_{sp}/\omega & \cdots & -\sum_{t \neq s} \nu_{st}/\omega \end{pmatrix},$$
(19)

and $[\rho]$ is the mass densities matrix

$$[\rho] = \begin{pmatrix} m_1 n_1 & & & & \\ & \ddots & & & \\ & & m_p n_p & & \\ & & & \ddots & \\ & & & m_s n_s \end{pmatrix}. \tag{20}$$

A. Parallel propagating waves in a collisionless plasma

In the absence of collisions ($[\nu] = 0$), the general dispersion relation of parallel wave propagation reduces to

$$\frac{1}{c^2} - \frac{k^2}{\omega^2} = \frac{\mu_0}{B_0^2} \sum_s \frac{\rho_s}{\omega^2 / \Omega_s^2 \pm \omega / \Omega_s}.$$
 (21)

"+" is for the R mode and "-" is for the L mode with respect to $\hat{B_0}$. The dispersion relation of parallel propagation of electromagnetic waves in collisionless plasma shown by Eq. (21) is consistent with those in previous works without considering the pressure of plasma. 24,25,27,28,37

We now study the properties of resonant and cutoff frequencies. For convenience of discussion, we treat wave frequency of the R mode as negative and frequency of the L mode as positive in a unified dispersion relation, by simply replacing "±" with "-" in Eq. (21). Then, we can rewrite Eq. (21) as

$$\frac{1}{c^2} - \frac{k^2}{\omega^2} = \frac{\mu_0}{B_0^2} \sum_s \rho_s \left(\frac{1}{\omega/\Omega_s - 1} - \frac{1}{\omega/\Omega_s} \right). \tag{22}$$

After applying the charge quasi-neutrality condition for the parallel propagating electromagnetic waves, $\sum_s \rho_s \Omega_s = \sum_s n_s q_s B_0 \approx 0$, we have

$$\frac{1}{c^2} - \frac{k^2}{\omega^2} = \frac{\mu_0}{B_0^2} \sum_s \frac{\rho_s}{\omega/\Omega_s - 1}.$$
 (23)

With the unified treatment of Eq. (23), the resonant frequencies are derived by setting $k^2 = \infty$. They occur at the gyrofrequencies of the charged species, $\omega_r = \Omega_s$, which is a well-known result. The cutoff frequencies, ω_c , can be derived, by setting k = 0, from

$$\sum_{s} \frac{\rho_{s}}{\omega_{c}/\Omega_{s} - 1} = \frac{B_{0}^{2}}{c^{2}\mu_{0}}.$$
 (24)

The left-hand-side of Eq. (24) is shown as the black solid curves, $F_1(\omega)$, and the right-hand-side of Eq. (24) is shown as the green solid line, $F_2(\omega)$. The cutoff frequencies, ω_c , occur where a black line intersects the green line. Figure 1 shows an example with two negatively charged species and three positively charged species when Eq. (24) is satisfied. The bottom panel of Fig. 1 illustrates the characteristic frequencies matched with those in the top panel, and the dispersion relation. For a particular wave mode, the L or R mode, there is a cutoff frequency that is higher (lower) than the corresponding gyrofrequency of ion (anion) species, and between two adjacent gyrofrequencies of ion species or anion species. In a relatively simple medium containing electrons and two ion species, the cutoff frequency between two gyrofrequencies of ions has been provided with simplifying approximations by 37

$$\omega_{cl} = \frac{c^2 |\Omega_{e^-}| \Omega_{a^+} \Omega_{b^+}}{V_A^2 (\omega_{pe^-}^2 + \omega_{pa^+}^2 + \omega_{pb^+}^2)},$$
 (25)

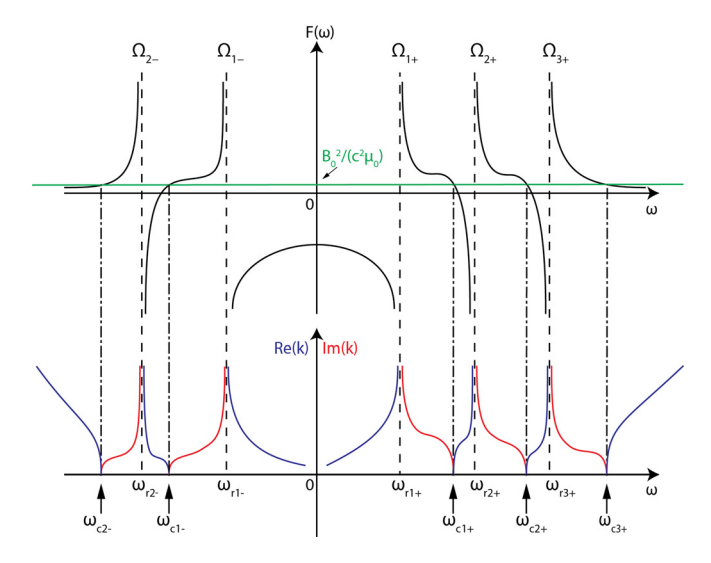


FIG. 1. Top panel: the solutions of cutoffs in Eq. (24) with the intersections between the black lines, $F_1(\omega) = \sum_s \frac{\rho_s}{\omega/\Omega_s-1}$, and the green line, $F_2(\omega) = \frac{B_0^2}{c^2\mu_0}$, in a medium consisting of three positively charged species and two negatively charged species; bottom panel: corresponding Re(k), blue lines, and Im(k), red lines, as functions of frequency ω . Waves propagate only in the blue line regions. Ω_s represents the gyrofrequencies of charged species, ω_r represents the resonant frequencies, and ω_c represents the cutoff frequencies.

where V_A is the Alfvén speed, $V_A = B_0/\sqrt{\mu_0\rho_{total}}$, and a and b denote the two ion species. For multiple species, Eq. (24) may not be solved for the cutoff frequencies in a general analytical form.

For a plasma containing electrons, when the absolute value of the upper cutoff frequency, $|\omega_{cu}|$, is about $|\Omega_{e^-}|$ and is much greater than the highest gyrofrequency of other charged species, rewriting Eq. (24) yields

$$\frac{\rho_{e^{-}}}{\omega_{cu}/\Omega_{s}-1} + \sum_{s \neq e^{-}} \rho_{s} \frac{\Omega_{s}}{\omega_{cu}} \left(1 - \frac{\Omega_{s}}{\omega_{cu}}\right)^{-1} = \frac{B_{0}^{2}}{c^{2}\mu_{0}}, \quad (26)$$

and then with Taylor expansion on $(1 - \Omega_s/\omega)^{-1}$ and neglecting the high order terms of Ω_s/ω , we have

$$\frac{\rho_{e^-}}{\omega_{cu}/\Omega_s - 1} + \sum_{s \neq e^-} \rho_s \frac{\Omega_s}{\omega_{cu}} \left(1 + \frac{\Omega_s}{\omega_{cu}} \right) = \frac{B_0^2}{c^2 \mu_0}.$$
 (27)

Applying the charge quasi-neutrality condition, $\rho_{e^-}\Omega_{e^-}+\sum_{s\neq e^-}\rho_s\Omega_s=\sum_s n_sq_sB_0\approx 0$, we have

$$\frac{\omega_{pe^{-}}^{2}}{\omega_{cu}(\omega_{cu} - \Omega_{e^{-}})} + \frac{1}{\omega_{cu}^{2}} \sum_{s \neq e^{-}} \omega_{ps}^{2} = 1.$$
 (28)

As the mass of an electron is much less than that of an ion, the ion plasma frequencies are much smaller than that of electrons. Therefore, we may neglect the second term in Eq. (28) and obtain the solution of the upper cutoff frequency as

$$\omega_{cu} = \pm \sqrt{\omega_{pe^{-}}^{2} + \Omega_{e^{-}}^{2}/4} - \Omega_{e^{-}}/2,$$
 (29)

where "–" is for the R mode and "+" is for the L mode. Notice that we treat the wave frequency of the R mode as negative. The solution of $|\omega_{cu}|$ is consistent with the

discussion of Ref. 38, of which the motions of ions are neglected for their large inertia. Then, the highest cutoff frequencies for both the L mode and the R mode are related to electron plasma frequency and therefore to the electron density. The properties of cutoffs will be discussed further with examples Secs. III B and IV.

B. Parallel propagating waves in a partially ionized collisional plasma

When magnetic perturbation propagates along the magnetic field line of force, neutral species will be driven by collisions between neutral species and charged species which oscillate with the magnetic field. Besides, the collisions between different charged species could make their responses to magnetic perturbations different from those in the collisionless case. In this section, we will discuss the processes of wave propagation in a collisional plasma with multiple species.

1. Simplifying approximations

In the general dispersion relation, in Eq. (17), wavenumber k is related to the magnitude of background magnetic field, collision frequencies, and densities of species. Stronger magnetic field indicates that the gyrofrequencies of charged species are higher and that the field lines are more rigid so that the perturbation propagates more quickly. Normalizing the wave frequency and collision frequencies with the gyrofrequency of a typical species, i.e., Ω_{O^+} , the effects of the magnitude of magnetic field on propagation are scaled to a reference field strength of Ω_{O^+} . To learn the effects of the magnetic field, we shall take it as constant and focus on the effects of collisions and densities.

In the dispersion relation in our 1-D (parallel propagation) model, temperature makes no effects on the wave propagation, even though it could affect the ionization fraction of medium and the collision frequencies. The ionization fraction, which may change with the temperature, can also be controlled by photoionization, ³⁹ as ionization can be produced by ionizing photons, the energies of which are not necessarily related to the local temperature. In our following discussion, we neglect the effects of temperature difference. Then, the collision frequencies are proportional to the densities directly.

To numerically study the effects of densities on wave propagation, we shall use a set of reference values, typical of the terrestrial ionosphere, and allow the densities of each species varying in large ranges around the reference values. Considering that the atmosphere of a planet, with greater (smaller) gravity compared to the Earth, can be denser (less dense) than that on the Earth, the concentration of each species can be very different. The densities of different species, because of different particle masses, may vary exponentially with the altitude relative to their corresponding scale heights. Since the ionization by photons can also vary in a large range depending on the radiative characteristic of the star it surrounds, the propagation can be studied not only in highly or weakly ionized medium but also in dense or tenuous plasma. In all, by adjusting densities of each species in the medium,

we can study the effects of concentrations of charged species, ion-ion collisions, ion-neutral collisions, and ionization on wave propagation, and characteristic frequencies such as resonant and cutoff frequencies.

Without losing the generality but with manageable complexity, we study wave propagation in a collisional plasma including four species, electrons, H^+ , O^+ , and neutrals, and focus on the L mode as there are two ion species. The neutrals may have different components but they are treated as a single species here. For a particular ion species, the ionneutral collision frequency is calculated by summing the collision frequencies between ions and each component of neutral species, and the neutral-ion collision frequency is calculated by the momentum conservation conditions. The magnetic field is assumed to be a constant and $B_0 = 0.6 \,\mathrm{G}$ corresponding to the Earth's polar ionospheric field and $\Omega_{O^+} \approx 358 \, \mathrm{s}^{-1}$. We use temperature $T = 800 \, \mathrm{K}$ to calculate the cross sections of collisions according to Ref. 36. The plasma densities are $N_{Ee^{-}} = N_{EH^{+}} + N_{EO^{+}} = 10^{4} \text{cm}^{-3}$, and the concentrations of H^+ and O^+ may be variable. The neutral density $\rho_n=2.66\times 10^{-15} {\rm g/cm^3}$ and the ionization fraction $\alpha\approx 10^{-4}$. The corresponding Alfvén speed is calculated by $V_A = B_0 / \sqrt{\mu_0 \sum_{s \neq n} \rho_s}$.

Figure 2 shows Re(k), column 1, Im(k), column 2, and phase velocity V_{ph} , column 3, as function of ω for the L mode in rows A, B, C, and D in which the percentage of H^+

species, the total density, the charged species density, and the neutral species density vary, respectively. In row A, the H^+ concentration varies from 0% to 100%; in rows B, C, and D, for $N_{H^+} = N_{O^+}$, the total density, the charged species density, and the neutral species density vary by orders of $10^{-1} - 10^{5}$ from those in row A which are set as reference values.

2. Results overview

In Fig. 2, when the densities of species are low, which indicates weaker collisions when the collision frequencies are less than the gyrofrequencies of ions, such as in row A and in the low density regions of $\rho/\rho_E \leq 10^3$, $\rho_i/\rho_{Ei} \leq 10^3$, and $\rho_n/\rho_{En} \leq 10^3$ in rows B, C, and D, respectively, four characteristic frequencies are shown in these panels. For example, in column 1, two resonant frequencies for O^+ and H^+ are shown, respectively, by the peaks with sharp color change at $\omega/\Omega_{O^+}=1$ and $\omega/\Omega_{H^+}=16$, and two cutoff frequencies are shown by the edges with sharp color change, of which the lower one, ω_{cl} , is between Ω_{O^+} and Ω_{H^+} and the upper one, ω_{cu} , is well above Ω_{H^+} .

There are two stopbands, from Ω_{O^+} to ω_{cl} and from Ω_{H^+} to ω_{cu} , in which the propagation is highly damped from column 2, while the phase velocities are faster than the speed of light from column 3 in which the panels are shown in 2-D plots. In the lower passband in which the wave frequency is

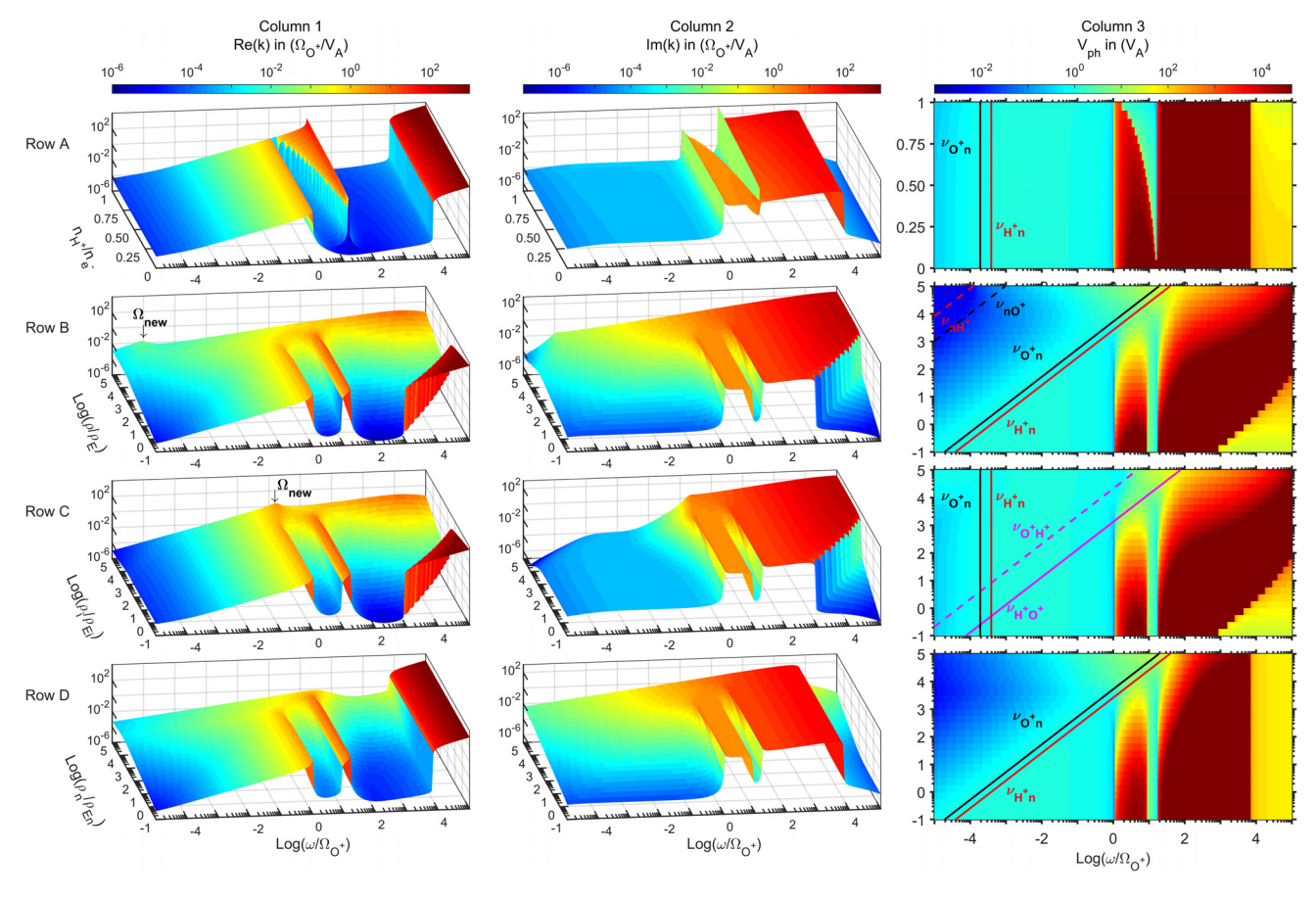


FIG. 2. Re(k) normalized by Ω_{O^+}/V_A , column 1, Im(k) normalized by Ω_{O^+}/V_A , column 2, and phase velocity V_{ph} normalized by V_A , column 3, as a function of ω for the Left-handed mode, assuming the plasma medium contains e^- , H^+ , O^+ , and neutral species. Row A is for the H^+ concentration varying from 0% to 100%. Rows B, C, and D are, respectively, for the total species ρ , charged species ρ_i , and neutral densities ρ_n , respectively, varying from that in row A with constant ion composition (50% H^+ and 50% O^+).

lower than Ω_{O^+} , the phase velocities are equal to the Alfvén speed in frequencies between the ion-neutral collision frequency and Ω_{O^+} . For a plasma with low ionization fraction, the ion-neutral collision frequency mentioned here is the maximum of the collision frequencies between each ion species with the neutral species, and the neutral-ion collision frequency mentioned here is the minimum of the collision frequencies between the neutral species with each ion species. Between the neutral-ion collision frequency and the ion-neutral collision frequency, the phase velocity decreases when the wave frequency decreases because of the neutral inertial loading. 40 Below the neutral-ion collision frequency, the phase velocity is constant and is lower than the Alfvén speed, indicating that the neutral species are completely driven by collisions. In the middle pass-band between ω_{cl} and Ω_{H^+} , the phase velocities are about the Alfvén speed, and in the upper pass-band in which the wave frequency is greater than ω_{cu} , the perturbations propagate as light waves and are not affected by collisions.

With a larger density, shown in high density regions of $\rho/\rho_E \geq 10^3$, $\rho_i/\rho_{Ei} \geq 10^3$, and $\rho_n/\rho_{En} \geq 10^3$ in rows B, C, and D, respectively, stronger collisions make it difficult for charged particles to complete gyromotions. Therefore, the resonances at Ω_{O^+} and Ω_{H^+} and lower cutoffs become weaker, shown by less precipitous edges with more gradual color changes. On the other hand, the change at the upper cutoffs is not as strong because ω_{cu} is so large compared with the collision frequencies that the waves do not feel any collisions in one wave period.

In rows B and C, ω_{cu} increases when the electron plasma frequency increases according to Eq. (29), forming a striking feature at the lower right corner. As the wave frequency is very large, much greater than the upper cutoff frequency as shown in Eq. (29) and collision frequencies, the charged particles do not feel any collisions or perturbations of fields in one wave period. Therefore, under such a situation, waves propagate similar to that in free space. In rows A and D, ω_{cu} remains the same when the electron density does not change.

3. Influence of the variable collision frequencies

In addition to these general features, here are also some detailed specific features and processes that are worth for indepth examinations. We now discuss the influence of the variables in each row. In row A, when H^+ concentration varies from 0% to 100% in the number density of ions, ω_{cl} decreases from Ω_{H^+} to Ω_{O^+} but ω_{cu} does not change. With a very small ionization fraction in this case, ion collision frequencies are much lower than the gyrofrequencies of O^+ and H^+ , shown in panel A3. Comparing to the collisionless case, the wave propagation is highly damped in the stopbands, shown in panel A2, with an extremely small but nonzero real part of wavenumber, shown in panel A1, and the phase velocity is faster than the speed of light which is shown at wave frequency greater than ω_{cu} in panel A3. When the wave frequency is between ν_{H^+n} and Ω_{O^+} , the phase velocity is equal to the Alfvén speed, which means that the wave propagation does not feel the existence of the neutral species because the neutral collision frequencies are lower than the wave frequency. Note that in panel A3, the phase velocity in frequencies between $0.1\Omega_{O^+}$ and Ω_{O^+} is slightly lower than that at frequencies between ν_{H^+n} and $0.1\Omega_{O^+}$. In the frequency range below Ω_{O^+} , the phase velocity decreases slightly from the Alfvén speed when the wave frequency increases and decreases severely to a lowest value at Ω_{O^+} . But the velocity change is negligible and we can still treat the phase velocity at frequencies between ν_{H^+n} and Ω_{O^+} as the Alfvén speed. In frequencies lower than ν_{H^+n} , the phase velocity decreases due to the neutral inertia loading, which indicates that the neutral species start gaining some appreciable portion of energy by collisions mainly with ions and being driven by magnetic perturbation.

In row B, when the total density increases (the concentrations of each species increase and the concentration ratios remain the same), the low cutoff frequency does not change according to Eq. (25), but the upper cutoff frequency increases according to Eq. (29). From panel B3, when the total density increases, the ion-neutral collision frequency increases and the frequency range in which the phase velocity equals the Alfvén speed becomes narrower. With very high total density $\rho/\rho_E \approx 10^5$, the collisions between ions and neutral species are very strong, and the resonance at Ω_{O^+} and Ω_{H^+} completely disappears, but there is a tendency for a new resonant frequency, Ω_{new} , to emerge, for example, the peak at about 10^{-4} of Ω_{O^+} in panel B1. Below Ω_{new} , the phase velocity is constant and about 100 times smaller than the Alfvén speed which indicates that the neutral species could be completely driven by magnetic field. This phase velocity equals the Alfvén speed when using the total mass density due to inertia loading, $V_{ph} = B_0 / \sqrt{\mu_0 \rho_{total}}$, as found by Ref. 40. When the collisions increase, the stopbands also change along with the disappearance of the resonances at Ω_{O^+} and Ω_{H^+} and emergence of the new resonant frequency. Basically, when the total density increases, the damping increases in $\nu_{in} \ll \omega \ll \Omega_{O^+}$, increases relatively slightly in $\nu_{ni} \ll \omega \ll \nu_{in}$, and decreases in $\omega \ll \nu_{ni}$, shown in panel B2 with a curved corner when $\rho/\rho_E \ge 10^5$. But if $\nu_{ni} \geq \Omega_{O^+}$, shown in the region where $\rho/\rho_E \geq 10^5$, the damping decreases in wave frequencies below Ω_{O^+} instead of ν_{ni} when the total density increases.

In row C, when the density of the charged species increases, the resonances at Ω_{O^+} and Ω_{H^+} become weaker, which is similar to that in row B. When the charged species density is large enough, i.e., $\rho_i/\rho_{Ei}\approx 10^5$, the collisions between O^+ and H^+ species are very strong, and a peak emerges at $\omega/\Omega_{O^+}\approx 10^{0.1}$ in panel C1. In the region of $\rho_i/\rho_{Ei}\approx 10^5$ in panel C3, at the wave frequency below Ω_{new} instead of Ω_{O^+} , the phase velocity equals the Alfvén speed. In wave frequencies between ν_{ni} and Ω_{O^+} , the damping, different from that in row B, does not change much when the charged species density increases. Since the neutral-ion collision frequencies are lower than the new emerged resonant frequency in this situation, the damping increases in wave frequencies between ν_{ni} and Ω_{O^+} and decreases in wave frequencies below ν_{ni} , shown at the top left corner in panel C2.

In row D, when the neutral density increases, the ionneutral collision frequency which is proportional to N_n increases but the neutral-ion collision frequency which is proportional to N_i keeps the same. The resonances at Ω_{H^+} and Ω_{O^+} disappear but there is no new resonant peak in panel D1. When $\rho_n/\rho_{En} \geq 10^4$, the phase velocity increases linearly when the wave frequency increases in the frequency range below ω_{cu} . The damping increases linearly in the frequency region below ω_{cu} , which is similar to that in row B except when $\rho_n/\rho_{En} \geq 10^4$.

4. Multi-species locked oscillation

In rows B and C of Fig. 2, the new resonant frequencies emerge when the collisions between charged species and neutral species, and between O^+ species and H^+ species, are strong enough, respectively. The strong collisions between two species or among more species could lock the oscillation of them and make them move together. Therefore, when the species are completely coupled, the new resonant frequency is related to the combined mass and charge of the species, written as

$$\Omega_{new} = \left(\sum_{s} n_{s} q_{s}\right) B / \left(\sum_{s} m_{s} n_{s}\right). \tag{30}$$

The coupling between plasma and neutral species by collisions plays an important role in affecting motion of plasma and could lower ion cyclotron frequency, 19,40,41 which is similar to the new resonant frequency discussed in Sec. III B 3. For a weakly ionized medium, the neutral-ion collision frequency is much lower than the ion-neutral collision frequency. We have shown that when the wave frequency is lower than the ion-neutral collision frequency, which is lower than the gyrofrequencies of ion species, the waves start to feel the existence of the neutrals so that the phase velocity is lower than the Alfvén speed due to the neutral inertia loading. When the wave frequency is lower than the neutral-ion collision frequency, the neutral species are completely driven by the collisions so that the propagation speeds of the perturbations of the neutral species and the plasma are the same and the corresponding Alfvén speed is calculated with the total density of medium. When the neutral-ion collision frequency is greater than Ω_{new} , there is a tendency to have a peak in the $Re(k) - \omega$ plot at the new resonant frequency. But this emerging peak is not as precipitous as that at Ω_{O^+} and Ω_{H^+} because the neutral species and the ion species are not at the same phase so that the rotating electric field cannot accelerate the combined species perfectly. Only when the new resonant frequency is much lower than the neutral-ion collision frequency, phase leading of the plasma is about zero so that the neutral species and the plasma can be treated as a single fluid and the peak could be more precipitous. This characteristic frequency can be seen in the dotted line, upper panel of Fig. 4 in Ref. 40. That is the case with heaviest collisions. From that figure, we see that the propagation velocity decreases significantly at $\alpha\Omega_i$, in which α denotes the ionization fraction and Ω_i denotes the gyrofrequency of ions. In collisional MHD, because of the collisions, which can cause a non-zero slippage between the motions of the plasmas and neutrals, one will not be able to obtain a solution with $k \to infinity$. Therefore, the propagation speed cannot go to zero, or in collisional MHD, the resonance condition does not coincide with the non-propagation condition. Mathematically, one may examine the dispersion relation (9) in Ref. 40. Letting $k \to infinity$ and ω finite, one would not be able to find frequencies that satisfy both the real and imaginary parts of the equation. More details of this process will be reported elsewhere.

IV. A SIMPLE CASE: WAVE PROPAGATION IN THE IONOSPHERE

We now apply our model to wave propagation in the terrestrial ionosphere. Based on the data from International Reference Ionosphere (IRI) and MISI-E-90 Atmosphere model at 0130 UT of January 1st, 2000, at 90° latitude, 45° longitude, we study wave propagation along the magnetic field from 100 km to 1000 km in the ionosphere with the general dispersion relation.

Ohms law, which provides the relationship between the current and electric field, has been derived under steady state assumption. In our case, this is the limit when the frequency goes to zero. The three-fluid case with one ion, one neutral, and one electron species has been discussed extensively by Refs. 40 and 42. In particular, the analysis of Ref. 42 shows that the Pedersen and Hall conductivities are dependent of frame of reference because the electric field depends on the frame of reference, but the current does not. In the example of the ionosphere, there are three possible frames of reference, the Earth frame, the neutral wind frame, and plasma frame. Therefore, a simple introduction of conductivities to correlate the current and electric field is problematic.

Figure 3 shows the altitude profiles of densities and temperatures of species (top panel), and of Alfvén speed and collision frequencies among the species (bottom panel). The magnitude of magnetic field is assumed as constant, B = 0.6 G. The plasma beta, the ratio of thermal and magnetic pressures, is estimated to about or less than 10^{-4} , which is much less than 1. Therefore, the medium can be approximated as cold plasma.

When electromagnetic perturbations propagate from the magnetopause or magnetotail to the ionosphere, the parallel incompressible Alfvénic (intermediate) mode wave is the most important for long-range coupling between two magnetically connected different media compared with the low frequency compressible fast mode, which is most effective in transferring energy in the latitudinal plane. In addition, when the perturbations propagate in a narrow direction, following the bending of the field lines, the power of the perturbations is more easily preserved even after a long distance, as for isotropic propagation the wave intensity may decrease with $1/r^2$. Therefore, with mutual coupling of various ion and neutral species via collisions, the incompressible waves may need to have a better description on the propagation and damping.

We make some simplifying assumptions to reduce the complexity of parameter-varying medium in our mathematical treatment but avoid losing much applicability. As we focus on the parallel propagation of incompressible waves,

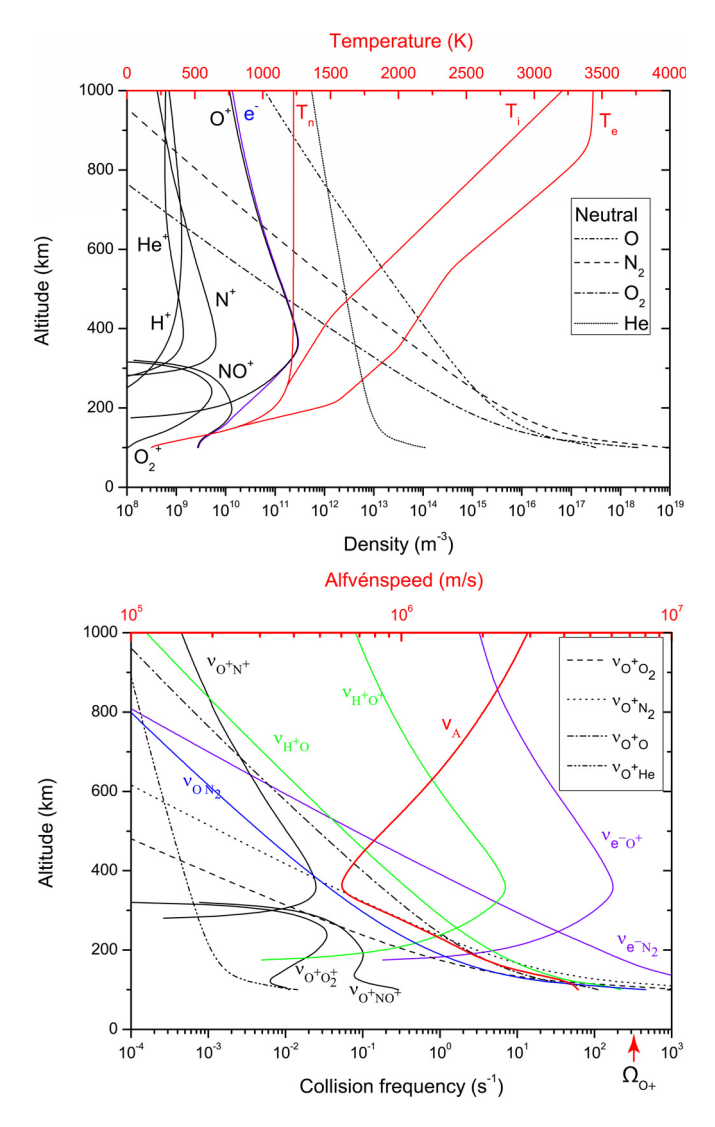


FIG. 3. Altitude profiles of species densities and temperatures (top panel), and of collision frequencies (not all are shown) and Alvén speed (bottom panel).

we assume that the magnetic field is vertically down to the ground, and the medium is stratified and locally uniform, of which the approximation is valid when the wavelength is much less than the gradient scale but may not be well suitable when the wave length is comparable to or longer than the scale length of the non-uniformity in the ionosphere. We ignore possible nonlinear coupling between shear Alfvén waves and slow MHD waves in a cold plasma.⁴⁴ We only consider that the wave propagates in the region where the net external forces and photochemical processes, and wave-particles interactions are negligible as they are beyond the scope of the present study. With these assumptions, the problem is reduced to a parallel propagation of electromagnetic waves in a locally uniform collisional cold plasma with multiple species. Even if some of the assumptions may be restrictive for some potential applications, the results of this study can still be used as a baseline to guide the understanding of the controlling processes for coupling of the magnetosphere with the ionosphere.

According to the data for each altitude in Fig. 3, we can calculate the real part and the imaginary part of the wavenumber k for the R mode and L mode through the general dispersion relation, Eq. (17), including all the multiple

species. Then, we calculate the phase velocity and the attenuation depth as functions of the wave frequency, from about 0.5 mHz to about 5 MHz, for the two wave modes and show them in Fig. 4. For Earth's field of 0.6 G, Ω_{O^+} is about 360 Hz, and we use this frequency to scale the wave frequencies. Note that because we do not solve a single wave propagation with height, the properties do not represent the time history of a wave propagating from either lower or higher altitude but represent the properties of propagation at each altitude. Furthermore, because there is a density gradient and the Alfvén speed changes with altitude, we employ the local uniform assumption according to which the wave propagation velocity equals the phase velocity evaluated using the local parameters.

In this section, we treat all the frequencies as positive. For the R mode in panel a1, there is a narrow stopband between Ω_{e^-} and the upper cutoff frequency of the R mode ω_{cu}^R . At frequencies greater than ω_{cu}^R , which is according to the electron density at each altitude, the phase velocity equals the speed of light, greenish in the color coding. If the wave is from the magnetosphere, propagating downward, the wave in the whole stopband range cannot reach the ground. Similarly, the waves from ground transmitters cannot reach space in this stopband along the magnetic field. In the frequency range between Ω_{O^+} and Ω_{e^-} , when the wave frequency increases, the phase velocity increases. This is the so called electron whistler mode.³⁸ In the frequency range below Ω_{O^+} , the phase velocity equals the Alfvén speed between the ion-neutral collision frequency and Ω_{O^+} . Similar to Sec. III B 2, the ionneutral collision frequency particularly represents the maximum collision frequencies between an ion species and a neutral species. Below the ion-neutral collision frequency, the phase velocity decreases when the wave frequency decreases because of the inertial loading of the neutral species. The R mode waves below Ω_{e^-} should be able to reach the ground. This is consistent with the fact that inter-hemispheric propagating whistler waves can be observed on the ground.

For the L mode in panel a2, the wide stopband at each altitude, from Ω_{O^+} to the upper cutoff frequency of the Left-handed wave, ω_{cu}^L , which is lower than ω_{cu}^R from Eq. (29), contains two very narrow passbands around Ω_{He^+} and Ω_{H^+} , clearly shown in panels a3 and a4, because of the existence of He^+ species above about 280 km and H^+ species above about 250 km. These two narrow passbands become wider at higher altitude because the concentration of H^+ and He^+ species becomes larger. However, the waves cannot propagate through the whole stopband from one side of the ionosphere to the other, from Ω_{O^+} to the peak of the ω_{cu}^L around the ionospheric peak height frequency. Reflection will occur on each side of the peak height. The L mode waves of magnetospheric origin should not be observed on the ground above Ω_{O^+} . If the waves are generated within the magnetosphere, e.g., at the plasmapause ($L \approx 4$), where the gyrofrequency of O^+ in Hz is $f_{O^+} \approx 360/(2\pi \times 4^3) \approx 1$ Hz. It is possible that the Pc waves, magnetospheric waves can interact with the electrons and ions of the magnetosphere, having an upper frequency limit of 1 Hz are due to this effect. 45,46

At about 100 km, the density of neutral species is so large that the ion-neutral collision frequencies are much larger than the gyrofrequencies of all individual ion species. Therefore, there are no resonances at the gyrofrequency of

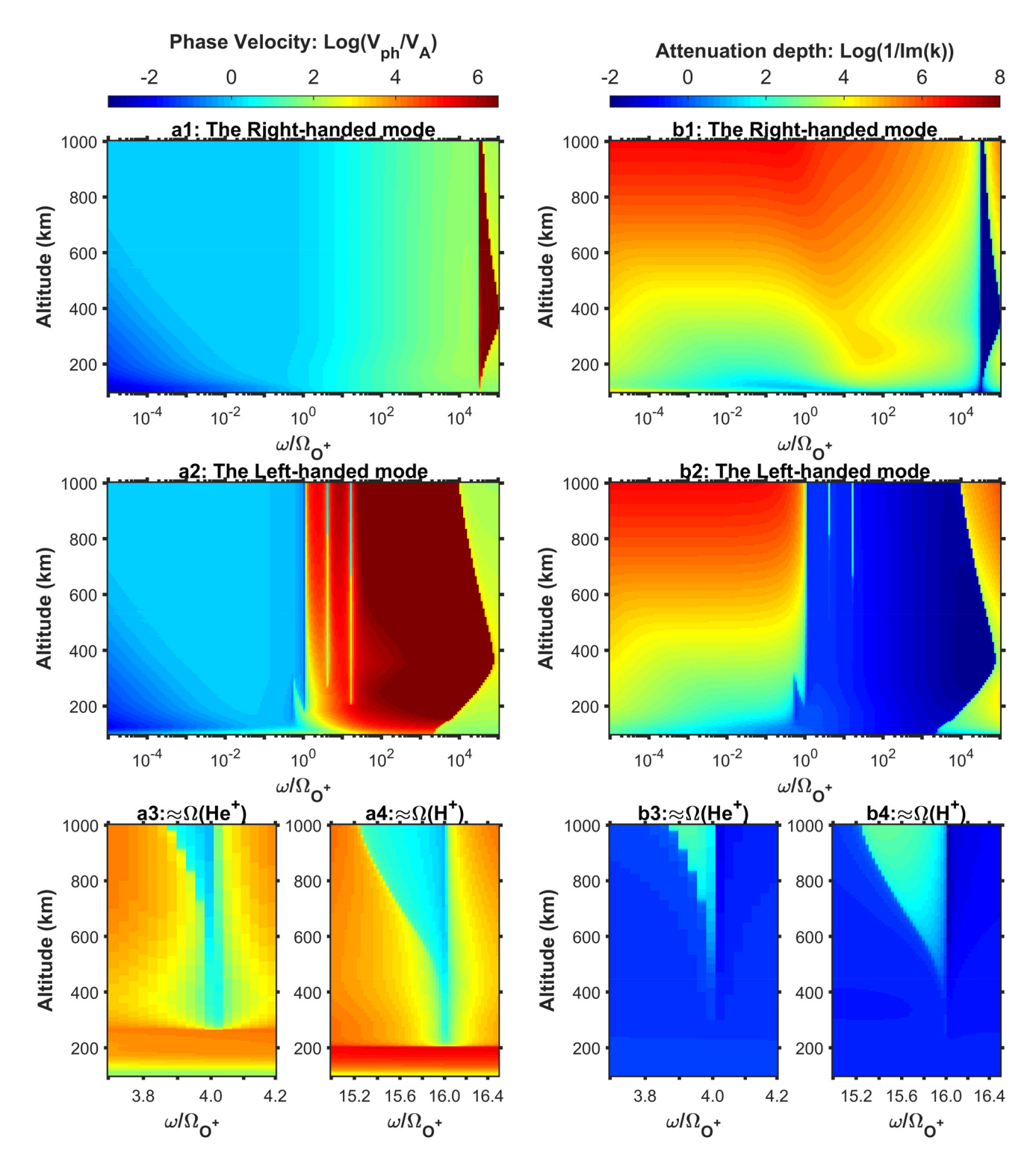


FIG. 4. Phase velocity, the left column, and attenuation depth, the right column, as functions of the wave frequency over 100 km-1000 km for the right-handed wave and the left-handed wave.

each ion species because collisions completely disrupt the gyromotion of charged particles. With very low ionization fraction, the neutral-ion collision frequency is much lower than the gyrofrequencies of all individual ion species. Between the neutral-ion collision frequency and the ionneutral collision frequency, the phase velocity decreases when the wave frequency decreases because of the inertia loading by neutral species. In the frequency range shown in the figures, the ion species and the neutral species do not act

as single fluid because of the very weak ionization. At altitudes from $100\,\mathrm{km}$ to about $150\,\mathrm{km}$, the neutral density decreases by 3 or 4 orders of that at $100\,\mathrm{km}$, when the ionneutral collision frequencies approach the resonant frequencies of O^+ and NO^+ which are the dominant species at this altitude so that the resonances by these two ions species start appearing. At altitudes from about $150\,\mathrm{km}$ to $300\,\mathrm{km}$, the neutral density decreases to one percent or one thousandth of that at $150\,\mathrm{km}$ so that the ion-neutral collision frequency

decreases rapidly and the ion-neutral collision frequencies become much lower than gyrofrequencies of ion species. The nearby resonant peaks of NO^+ and O_2^+ are so close that they could merge because of collisions. The resonant peak of O^+ appears above about 180 km, but the resonance of N^+ is not visible in the figure because Ω_{N^+} is so close to Ω_{O^+} . At altitudes above 320 km, NO^+ and O_2^+ are essentially absent and O^+ is the dominant ion species with small fractions (0%-10%) of H^+ and He^+ . With much lower collision frequencies at high altitudes, there are resonant frequencies at the gyrofrequencies of H^+ and He^+ , shown as the thin ridges in Fig. 4; even concentrations of H^+ and He^+ are low.

The attenuation depth, shown in the right column of Fig. 4, represents the absolute distance over which the wave amplitude decreases by a factor 1/e, regardless of wavelength. For the right-handed wave shown in panel b1, the attenuation depth is extremely small in the stopband. In the frequency range of the electron whistler mode, the attenuation depth becomes larger at higher frequency in general. For a particular wave frequency of the electron whistler mode, the attenuation depth becomes smaller with denser electron density. At about 400 km, because the electron density is largest, the width of green is largest. At about 100 km, the collisions are so strong that the attenuation depth is shorter than that at different altitudes in general. In the frequency range lower than Ω_{O^+} , there is a thin layer at about 100 km in which the ion-neutral collision frequency is greater than the Ω_{NO^+} that is the dominant ion species at this altitude. Because of the strong collisions, effects of the motions of charged species are relatively weak and then the attenuation depth more likely linearly increases when the wave frequency increases. The attenuation depth, above this thin layer, is generally greater at higher altitude. At the same altitude, the attenuation depth is about the same at wave frequencies greater than the ion-neutral collision frequency. According to the discussion in Sec. III B 3, the attenuation depth, at the same altitude, is greater when $\omega \leq \nu_{in}$ than that when $\omega \geq \nu_{in}$. Therefore, in Fig. 4, the color curves occur on the line of the ion-neutral collision frequency. Compared with that at altitude about 150 km, the attenuation depth in the thin layer at 100 km is greater in the frequency range below gyrofrequencies of ions, and is smaller in the frequency range between Ω_{O^+} and Ω_{e^-} . Therefore, in panel b1, there is a small blue region around 150 km at $\omega/\Omega_{O^+} = 10^{-2} - 10^0$, in which the attenuation depth is smallest.

For the left-handed wave shown in panel b2, in the stopband the attenuation depth is very small, and in the two passbands related to the He^+ and H^+ species, shown in panel b3 and b4, the attenuation depth is relatively large. In frequencies below Ω_{O^+} , the attenuation depth above 200 km is similar to that of the right-handed wave. Below about 150 km, the ionneutral collision frequency is very strong and the neutral-ion collision frequency is very small so that in the frequency range between these two collision frequencies, the attenuation depth decreases linearly when the wave frequency decreases.

V. SUMMARY AND DISCUSSION

Based on the multi-fluid treatment and the collision theory, we have derived a general dispersion relation for electromagnetic waves (or incompressible waves neglecting thermal pressure) propagating along the background magnetic field in a uniform partially ionized plasma with multiple species. This general dispersion relation can cover a board frequency range from MHD waves to light waves, and can include arbitrary number of positively charged or negatively charged species as well as neutral species.

In collisionless cases, by neglecting the collision terms in our dispersion relation, we get the same conclusions with previous works. There are the same number of resonant frequencies, cutoff frequencies, and stopbands with that of charged species. The resonant frequencies are at the gyrofrequencies of charged species. The lower cutoff frequencies between the gyrofrequencies of ions do not change when the concentrations of species do not change even though the concentrations vary. The upper cutoff frequencies for a medium containing electrons are related to the density of electrons.

The collisions between two species contribute to the coupling process of them. Under the weak collision condition, in which collision frequencies are smaller than the absolute value of gyrofrequencies of charged species, the resonance at the gyrofrequencies of charged species is weaker than that in the collisionless situation. In the stopbands, wave propagates with an extremely fast phase velocity and with strong damping that can be calculated quantitatively from the general dispersion relation. In general, the collisions between the charged species with the neutral species contribute to the damping more than the collisions among the charged species. When the ion-neutral collision frequency increases, the damping increases in frequencies between the ion-neutral collision frequency and the minimum gyrofrequency of ions, increases relatively slightly in frequencies between the neutral-ion collision frequency and the ionneutral collision frequency, and decreases in frequency under the neutral-ion collision frequency. Under the stronger collision conditions, species will couple more tightly so that a new resonant frequency, depending on the total charges and total mass of coupled species, may merge when the collision frequencies are greater than the new emerge resonant frequency.

We have also applied the general dispersion relation to study the propagation of incompressible waves from $100 \,\mathrm{km}$ to $1000 \,\mathrm{km}$ altitude of the ionosphere. Although we made several simplifying assumptions, the dispersion relation illustrated some properties related to the multiple species and collisions reasonably, especially when the wavelength is shorter than the gradient scale of ionosphere parameters. The features of phase velocity and attenuation depth at each altitude are clearly shown. In general, the phase velocity is slower than the Alfvén speed because of the inertia loading of neutral species in the frequency range between neutral-ion collision frequency and ion-neutral collision frequency, which occurs at wave frequency lower than the gyrofrequency of O^+ . The attenuation depth is lower at lower altitude with stronger collisions in the passbands of both L mode and R mode waves.

ACKNOWLEDGMENTS

This work was supported by NASA Grant No. NNX12AD22G and NSF Grant Nos. AGS-1559717, AGS-1702134, and AGS-0903777.

APPENDIX: DERIVATION OF THE GENERALIZED DISPERSION RELATION WITH FOUR SPECIES

The coefficient matrix in Eq. (16)

$$[A] = \begin{pmatrix} if_1 + X_1 - \frac{\omega_{p1}^2}{K^2} & -if_{12} - \frac{\Omega_1 \omega_{p2}^2}{\Omega_2 K^2} & -if_{13} - \frac{\Omega_1 \omega_{p3}^2}{\Omega_3 K^2} & -if_{14} - \frac{\Omega_1 \omega_{p4}^2}{\Omega_4 K^2} \\ -if_{21} - \frac{\Omega_2 \omega_{p1}^2}{\Omega_1 K^2} & if_2 + X_2 - \frac{\omega_{p2}^2}{K^2} & -if_{23} - \frac{\Omega_2 \omega_{p3}^2}{\Omega_3 K^2} & -if_{24} - \frac{\Omega_2 \omega_{p4}^2}{\Omega_4 K^2} \\ -if_{31} - \frac{\Omega_3 \omega_{p1}^2}{\Omega_1 K^2} & -if_{32} - \frac{\Omega_3 \omega_{p2}^2}{\Omega_2 K^2} & if_3 + X_3 - \frac{\omega_{p3}^2}{K^2} & -if_{34} - \frac{\Omega_3 \omega_{p4}^2}{\Omega_4 K^2} \\ -if_{41} - \frac{\Omega_4 \omega_{p1}^2}{\Omega_1 K^2} & -if_{42} - \frac{\Omega_4 \omega_{p2}^2}{\Omega_2 K^2} & -if_{43} - \frac{\Omega_4 \omega_{p3}^2}{\Omega_3 K^2} & if_4 + X_4 - \frac{\omega_{p4}^2}{K^2} \end{pmatrix},$$
(A1)

where $\Omega_s = q_s B_0/m_s$ and $\omega_{ps} = \sqrt{n_s q_s^2/(\varepsilon_0 m_s)}$ are the cyclotron frequency and plasma frequency, respectively, of species s, $\nu_s = \sum_{t \neq s} \nu_{st}$, $K^2 = -c^2 k^2 + \omega^2$, $X_s = 1 - i\Theta\Omega_s/\omega$, $f_{st} = \nu_{st}/\omega$. The determinant of matrix [A] in Eq. (A1) must be zero to obtain nontrivial solutions. Here, we use 4 species to illustrate the derivation which can be extended to an arbitrary number of

species. Construct a matrix whose determinant is $1 \ [P] = \begin{pmatrix} 1 & -\frac{Q_2}{Q_1} & -\frac{Q_3}{Q_1} & -\frac{Q_4}{Q_1} \\ 0 & 1 & 0 & 0 \\ 0 & 0 & 1 & 0 \\ 0 & 0 & 0 & 1 \end{pmatrix}$. Here $Q_i = q_i n_i$. From the product the-

orem of matrix [Arfken, Weber 2006], we have |A||P| = |AP|. Then

$$\begin{vmatrix} if_{1} + X_{1} - \frac{\omega_{p1}^{2}}{K^{2}} & -if_{12} - \frac{Q_{2}}{Q_{1}}(f_{1} + X_{1}) & -if_{13} - \frac{Q_{3}}{Q_{1}}(f_{1} + X_{1}) & -if_{14} - \frac{Q_{4}}{Q_{1}}(f_{1} + X_{1}) \\ -if_{21} - \frac{\Omega_{2}\omega_{p1}^{2}}{\Omega_{1}K^{2}} & if_{2} + X_{2} - \frac{Q_{2}}{Q_{1}}(-if_{21}) & -if_{23} - \frac{Q_{3}}{Q_{1}}(-if_{21}) & -if_{24} - \frac{Q_{4}}{Q_{1}}(-if_{21}) \\ -if_{31} - \frac{\Omega_{3}\omega_{p1}^{2}}{\Omega_{1}K^{2}} & -if_{32} - \frac{Q_{2}}{Q_{1}}(-if_{31}) & if_{3} + X_{3} - \frac{Q_{3}}{Q_{1}}(-if_{31}) & -if_{34} - \frac{Q_{4}}{Q_{1}}(-if_{31}) \\ -if_{41} - \frac{\Omega_{4}\omega_{p1}^{2}}{\Omega_{1}K^{2}} & -if_{42} - \frac{Q_{2}}{Q_{1}}(-if_{41}) & -if_{43} - \frac{Q_{3}}{Q_{1}}(-if_{41}) & if_{4} + X_{4} - \frac{Q_{4}}{Q_{1}}(-if_{41}) \end{vmatrix} = 0.$$
(A2)

Decompose the determinant related to the first column into two terms

$$\begin{vmatrix} if_1 + X_1 & -if_{12} - \frac{Q_2}{Q_1}(f_1 + X_1) & -if_{13} - \frac{Q_3}{Q_1}(f_1 + X_1) & -if_{14} - \frac{Q_4}{Q_1}(f_1 + X_1) \\ -if_{21} & if_2 + X_2 - \frac{Q_2}{Q_1}(-if_{21}) & -if_{23} - \frac{Q_3}{Q_1}(-if_{21}) & -if_{24} - \frac{Q_4}{Q_1}(-if_{21}) \\ -if_{31} & -if_{32} - \frac{Q_2}{Q_1}(-if_{31}) & if_3 + X_3 - \frac{Q_3}{Q_1}(-if_{31}) & -if_{34} - \frac{Q_4}{Q_1}(-if_{31}) \\ -if_{41} & -if_{42} - \frac{Q_2}{Q_1}(-if_{41}) & -if_{43} - \frac{Q_3}{Q_1}(-if_{41}) & if_4 + X_4 - \frac{Q_4}{Q_1}(-if_{41}) \\ \end{vmatrix} - \frac{\omega_{p1}^2}{K^2} & -if_{12} - \frac{Q_2}{Q_1}(f_1 + X_1) & -if_{13} - \frac{Q_3}{Q_1}(f_1 + X_1) & -if_{14} - \frac{Q_4}{Q_1}(f_1 + X_1) \\ - \frac{\Omega_2\omega_{p1}^2}{\Omega_1K^2} & if_2 + X_2 - \frac{Q_2}{Q_1}(-if_{21}) & -if_{23} - \frac{Q_3}{Q_1}(-if_{21}) & -if_{24} - \frac{Q_4}{Q_1}(-if_{21}) \\ - \frac{\Omega_3\omega_{p1}^2}{\Omega_1K^2} & -if_{32} - \frac{Q_2}{Q_1}(-if_{31}) & if_3 + X_3 - \frac{Q_3}{Q_1}(-if_{31}) & -if_{34} - \frac{Q_4}{Q_1}(-if_{31}) \\ - \frac{\Omega_4\omega_{p1}^2}{\Omega_1K^2} & -if_{42} - \frac{Q_2}{Q_1}(-if_{41}) & -if_{43} - \frac{Q_3}{Q_1}(-if_{41}) & if_4 + X_4 - \frac{Q_4}{Q_1}(-if_{41}) \end{vmatrix} = 0.$$
(A3)

For the first term in (A3), we perform a reverse operation of [P], multiplying $[P]^{-1}$ on the right side, to obtain

$$\begin{vmatrix} if_1 + X_1 & -if_{12} & -if_{13} & -if_{14} \\ -if_{21} & if_2 + X_2 & -if_{23} & -if_{24} \\ -if_{31} & -if_{32} & if_3 + X_3 & -if_{34} \\ -if_{41} & -if_{42} & -if_{43} & if_4 + X_4 \end{vmatrix}.$$
(A4)

For the second term, collect the factor $-\frac{c^2\mu_0}{K^2B_0}Q_1$ in the first column to get

$$-\frac{c^{2}\mu_{0}}{K^{2}B_{0}}Q_{1} \cdot \begin{vmatrix} \Omega_{1} & -if_{12} - \frac{Q_{2}}{Q_{1}}(f_{1} + X_{1}) & -if_{13} - \frac{Q_{3}}{Q_{1}}(f_{1} + X_{1}) & -if_{14} - \frac{Q_{4}}{Q_{1}}(f_{1} + X_{1}) \\ \Omega_{2} & if_{2} + X_{2} - \frac{Q_{2}}{Q_{1}}(-if_{21}) & -if_{23} - \frac{Q_{3}}{Q_{1}}(-if_{21}) & -if_{24} - \frac{Q_{4}}{Q_{1}}(-if_{21}) \\ \Omega_{3} & -if_{32} - \frac{Q_{2}}{Q_{1}}(-if_{31}) & if_{3} + X_{3} - \frac{Q_{3}}{Q_{1}}(-if_{31}) & -if_{34} - \frac{Q_{4}}{Q_{1}}(-if_{31}) \\ \Omega_{4} & -if_{42} - \frac{Q_{2}}{Q_{1}}(-if_{41}) & -if_{43} - \frac{Q_{3}}{Q_{1}}(-if_{41}) & if_{4} + X_{4} - \frac{Q_{4}}{Q_{1}}(-if_{41}) \end{vmatrix}.$$
(A5)

Then, decomposing it related to the first column, we have

$$-\frac{c^{2}\mu_{0}}{K^{2}B_{0}}Q_{1} \cdot \begin{cases} if_{2} + X_{2} - \frac{Q_{2}}{Q_{1}}(-if_{21}) & -if_{23} - \frac{Q_{3}}{Q_{1}}(-if_{21}) & -if_{24} - \frac{Q_{4}}{Q_{1}}(-if_{21}) \\ -if_{32} - \frac{Q_{2}}{Q_{1}}(-if_{31}) & if_{3} + X_{3} - \frac{Q_{3}}{Q_{1}}(-if_{31}) & -if_{34} - \frac{Q_{4}}{Q_{1}}(-if_{31}) \\ -if_{42} - \frac{Q_{2}}{Q_{1}}(-if_{41}) & -if_{43} - \frac{Q_{3}}{Q_{1}}(-if_{41}) & if_{4} + X_{4} - \frac{Q_{4}}{Q_{1}}(-if_{41}) \end{cases} \\ -\Omega_{2} \cdot \begin{vmatrix} -if_{12} - \frac{Q_{2}}{Q_{1}}(f_{1} + X_{1}) & -if_{13} - \frac{Q_{3}}{Q_{1}}(f_{1} + X_{1}) & -if_{14} - \frac{Q_{4}}{Q_{1}}(f_{1} + X_{1}) \\ -if_{32} - \frac{Q_{2}}{Q_{1}}(-if_{31}) & if_{3} + X_{3} - \frac{Q_{3}}{Q_{1}}(-if_{31}) & -if_{34} - \frac{Q_{4}}{Q_{1}}(-if_{31}) \\ -if_{42} - \frac{Q_{2}}{Q_{1}}(-if_{41}) & -if_{43} - \frac{Q_{3}}{Q_{1}}(-if_{41}) & if_{4} + X_{4} - \frac{Q_{4}}{Q_{1}}(-if_{41}) \end{vmatrix} + (...) \end{cases}$$
(A6)

For simplicity, Eq. (A6) is not completely shown. A trick is rewriting (A6) as

$$-\frac{c^{2}\mu_{0}}{K^{2}B_{0}} \cdot \begin{cases} Q_{1} & Q_{2} - \frac{Q_{2}}{Q_{1}}Q_{1} & Q_{3} - \frac{Q_{3}}{Q_{1}}Q_{1} & Q_{4} - \frac{Q_{4}}{Q_{1}}Q_{1} \\ -if_{21} & if_{2} + X_{2} - \frac{Q_{2}}{Q_{1}}(-if_{21}) & -if_{23} - \frac{Q_{3}}{Q_{1}}(-if_{21}) & -if_{24} - \frac{Q_{4}}{Q_{1}}(-if_{21}) \\ -if_{31} & -if_{32} - \frac{Q_{2}}{Q_{1}}(-if_{31}) & if_{3} + X_{3} - \frac{Q_{3}}{Q_{1}}(-if_{31}) & -if_{34} - \frac{Q_{4}}{Q_{1}}(-if_{31}) \\ -if_{41} & -if_{42} - \frac{Q_{2}}{Q_{1}}(-if_{41}) & -if_{43} - \frac{Q_{3}}{Q_{1}}(-if_{41}) & if_{4} + X_{4} - \frac{Q_{4}}{Q_{1}}(-if_{41}) \end{cases} \\ +\Omega_{2} \cdot \begin{cases} f_{1} + X_{1} & -if_{12} - \frac{Q_{2}}{Q_{1}}(f_{1} + X_{1}) & -if_{13} - \frac{Q_{3}}{Q_{1}}(f_{1} + X_{1}) & -if_{14} - \frac{Q_{4}}{Q_{1}}(f_{1} + X_{1}) \\ Q_{1} & Q_{2} - \frac{Q_{2}}{Q_{1}}Q_{1} & Q_{3} - \frac{Q_{3}}{Q_{1}}Q_{1} & Q_{4} - \frac{Q_{4}}{Q_{1}}Q_{1} \\ -if_{31} & -if_{32} - \frac{Q_{2}}{Q_{1}}(-if_{31}) & if_{3} + X_{3} - \frac{Q_{3}}{Q_{1}}(-if_{31}) & -if_{34} - \frac{Q_{4}}{Q_{1}}(-if_{31}) \\ -if_{41} & -if_{42} - \frac{Q_{2}}{Q_{1}}(-if_{41}) & -if_{43} - \frac{Q_{3}}{Q_{1}}(-if_{41}) & if_{4} + X_{4} - \frac{Q_{4}}{Q_{1}}(-if_{41}) \end{cases} \end{cases} \right\}.$$
(A7)

Again, (A7) is not shown completely. Notice that the sign in front of Ω_2 is now positive. Perform reverse operation $[P]^{-1}$ on the right side to each term in (A7), similar to (A4). Then, combine (A5) and (A7)

$$\begin{vmatrix} if_{1} + X_{1} & -if_{12} & -if_{13} & -if_{14} \\ -if_{21} & if_{2} + X_{2} & -if_{23} & -if_{24} \\ -if_{31} & -if_{32} & if_{3} + X_{3} & -if_{34} \\ -if_{41} & -if_{42} & -if_{43} & if_{4} + X_{4} \end{vmatrix} = \frac{c^{2}\mu_{0}}{K^{2}B_{0}} \cdot \begin{cases} \Omega_{1} \cdot \begin{vmatrix} Q_{1} & Q_{2} & Q_{3} & Q_{4} \\ -if_{21} & if_{2} + X_{2} & -if_{23} & -if_{24} \\ -if_{31} & -if_{32} & if_{3} + X_{3} & -if_{34} \\ -if_{41} & -if_{42} & -if_{43} & if_{4} + X_{4} \end{vmatrix} + (\ldots) \end{cases}$$

$$+\Omega_{2} \cdot \begin{vmatrix} f_{1} + X_{1} & -if_{12} & -if_{13} & -if_{14} \\ Q_{1} & Q_{2} & Q_{3} & Q_{4} \\ -if_{31} & -if_{32} & if_{3} + X_{3} & -if_{34} \\ -if_{41} & -if_{42} & -if_{43} & if_{4} + X_{4} \end{vmatrix} + (\ldots) \end{cases} . \tag{A8}$$

$$\frac{(-c^2k^2 + \omega^2)B_0}{c^2\mu_0} = \begin{pmatrix} \Omega_1 & \Omega_2 & \Omega_3 & \Omega_4 \end{pmatrix} \begin{pmatrix} D_1 \\ D_2 \\ D_3 \\ D_4 \end{pmatrix}, \quad (A9)$$

where $(D_1 \quad D_2 \quad D_3 \quad D_4)^T$ satisfy

$$\begin{pmatrix} if_{1} + X_{1} & -if_{12} & -if_{13} & -if_{14} \\ -if_{21} & if_{2} + X_{2} & -if_{23} & -if_{24} \\ -if_{31} & -if_{32} & if_{3} + X_{3} & -if_{34} \\ -if_{41} & -if_{42} & -if_{43} & if_{4} + X_{4} \end{pmatrix}^{T}$$

$$\times \begin{pmatrix} D_{1} \\ D_{2} \\ D_{3} \\ D_{4} \end{pmatrix} = \begin{pmatrix} Q_{1} \\ Q_{2} \\ Q_{3} \\ Q_{4} \end{pmatrix}. \tag{A10}$$

Then, we can rewrite Eq. (A9) to obtain the final dispersion

$$\begin{split} &\frac{(-c^{2}k^{2}+\omega^{2})B_{0}}{c^{2}\mu_{0}} \\ &= \left(\Omega_{1} \quad \Omega_{2} \quad \Omega_{3} \quad \Omega_{4}\right) \\ &\times \left(\begin{pmatrix} if_{1}+X_{1} & -if_{12} & -if_{13} & -if_{14} \\ -if_{21} & if_{2}+X_{2} & -if_{23} & -if_{24} \\ -if_{31} & -if_{32} & if_{3}+X_{3} & -if_{34} \\ -if_{41} & -if_{42} & -if_{43} & if_{4}+X_{4} \end{pmatrix}^{T}\right)^{-1} \\ &\times \begin{pmatrix} Q_{1} \\ Q_{2} \\ Q_{3} \\ Q_{4} \end{pmatrix}. \end{split} \tag{A11}$$

Equation (A11) is in its general form, which can be rewritten in the same form as shown in Eq. (17).

¹⁰R. Soler, R. Oliver, and J. Ballester, Astrophys. J. 707, 662 (2009).

¹¹W. Gekelman, S. Vincena, and D. Leneman, Plasma Phys. Controlled Fusion 39, A101 (1997).

¹²G. Gnavi, R. Galvão, F. Gratton, and L. Gomberoff, Phys. Rev. E **54**, 4112

¹³W. Pilipp, T. Hartquist, O. Havnes, and G. Morfill, Astrophys. J. 314, 341 (1987).

¹⁴N. Cramer and S. Vladimirov, Phys. Plasmas 3, 4740 (1996).

¹⁵M. Hertzberg, N. Cramer, and S. Vladimirov, Phys. Rev. E 69, 056402

¹⁶J. E. Leake and T. Arber, Astron. Astrophys. **450**, 805 (2006).

¹⁷T. D. Arber, M. Haynes, and J. E. Leake, Astrophys. J. **666**, 541 (2007).

¹⁸R. Soler, R. Oliver, and J. Ballester, Astrophys. J. **699**, 1553 (2009).

¹⁹B. P. Pandey and M. Wardle, Mon. Not. R. Astron. Soc. **385**, 2269 (2008). ²⁰T. V. Zaqarashvili, M. L. Khodachenko, and H. O. Rucker, Astron. Astrophys. **529**, A82 (2011); e-print arXiv:1101.3913 [astro-ph.SR].

²¹D. Martínez-Gómez, R. Soler, and J. Terradas, Astrophys. J. **837**, 80 (2017).

²²S. Buchsbaum, Phys. Rev. Lett. **5**, 495 (1960).

²³S. Buchsbaum, Phys. Fluids **3**, 418 (1960).

²⁴R. L. Smith and N. Brice, J. Geophys. Res. 69, 5029, https://doi.org/ 10.1029/JZ069i023p05029 (1964).

²⁵T. Boyd and J. Sanderson, *Plasma Dynamics*, Applications of Mathematics Series (Barnes & Noble, New York, NY, 1969).

²⁶T. H. Stix, Waves in Plasmas (American Institute of Physics, College Park, MD, 1992), p. 566.

²⁷W. Baumjohann and R. Treumann, Basic Space Plasma Physics (Imperial College Press, London, UK, 1997).

²⁸N. F. Cramer, *The Physics of Alfvén Waves* (Wiley-VCH, Weinheim, Germany, 2011).

²⁹P. L. Auer, H. Hurwitz, and R. D. Miller, *Phys. Fluids* **1**, 501 (1958).

³⁰K. Rahbarnia, S. Ullrich, K. Sauer, O. Grulke, and T. Klinger, Phys. Plasmas 17, 032102 (2010).

³¹S. T. Vincena, G. J. Morales, and J. E. Maggs, Phys. Plasmas 17, 052106 (2010).

³²J. R. Johnson and C. Cheng, Geophys. Res. Lett. 26, 671, https://doi.org/ 10.1029/1999GL900074 (1999).

³³E.-H. Kim, J. R. Johnson, and D.-H. Lee, J. Astron. Space Sci. 32, 289

³⁴D. Bilitza, D. Altadill, Y. Zhang, C. Mertens, V. Truhlik, P. Richards, L.-A. McKinnell, and B. Reinisch, J. Space Weather Space Clim. 4, A07

³⁵A. E. Hedin, J. Geophys. Res.: Space Phys. **96**, 1159, https://doi.org/ 10.1029/90JA02125 (1991).

³⁶R. Schunk and A. Nagy, Ionospheres: Physics, Plasma Physics, and Chemistry, 2nd ed., Cambridge Atmospheric and Space Science Series (Cambridge University Press, Cambridge, UK, 2009).

³⁷S. Irie and Y. Ohsawa, J. Phys. Soc. Jpn. **70**, 1585 (2001).

³⁸C. Russell, J. Luhmann, and R. Strangeway, *Space Physics: An* Introduction (Cambridge University Press, Cambridge, UK, 2016).

³⁹J. Berkowitz, *Photoabsorption*, *Photoionization*, and *Photoelectron* Spectroscopy (Academic Press, Cambridge, MA, 2012).

⁴⁰P. Song, V. Vasyliūnas, and L. Ma, J. Geophys. Res.: Space Phys. 110(A9), A09309, https://doi.org/10.1029/2005JA011139 (2005).

⁴¹P. M. Bellan, Plasma Phys. Controlled Fusion **60**, 014006 (2018).

⁴²P. Song, T. Gombosi, and A. Ridley, J. Geophys. Res.: Space Phys. 106, 8149, https://doi.org/10.1029/2000JA000423 (2001).

⁴³B. Reinisch, X. Huang, P. Song, G. Sales, S. Fung, J. Green, D. Gallagher, and V. Vasyliunas, Geophys. Res. Lett. 28, 4521, https://doi.org/10.1029/ 2001GL013684 (2001).

⁴⁴A. Streltsov, J. Geophys. Res.: Space Phys. **116**(A10), A10203, https:// doi.org/10.1029/2011JA016550 (2011).

⁴⁵R. E. Erlandson and B. J. Anderson, J. Geophys. Res.: Space Phys. **101**, 7843, https://doi.org/10.1029/96JA00082 (1996).

⁴⁶K. Mursula, J. Atmos. Sol.-Terr. Phys. **69**, 1623 (2007).

⁴⁷G. Arfken, H. Weber, and F. Harris, *Mathematical Methods for Physicists:* A Comprehensive Guide (Academic Press, Cambridge, MA, 2011).

¹C. K. Goertz and R. W. Boswell, J. Geophys. Res.: Space Phys. 84, 7239, https://doi.org/10.1029/JA084iA12p07239 (1979).

²R. L. Lysak, Space Sci. Rev. **52**, 33 (1990).

³M. G. Kivelson and C. T. Russell, Introduction to Space Physics (Cambridge University Press, Cambridge, UK, 1995).

⁴P. Song and V. Vasyliūnas, J. Geophys. Res.: Space Phys. 107, SMP 11-1-SMP11-8, https://doi.org/10.1029/2002JA009364 (2002).

⁵P. Song and V. Vasyliūnas, Geophys. Monogr. Ser. **201**, 201–215, https:// doi.org/10.1029/2012GM001308 (2013).

⁶W. Lotko, J. Atmos. Sol.-Terr. Phys. **66**, 1443 (2004).

⁷J. Tu and P. Song, J. Geophys. Res.: Space Phys. 121, 11,861, https:// doi.org/10.1002/2016JA023393 (2016).

⁸D. B. Jess, M. Mathioudakis, R. Erdélyi, P. J. Crockett, F. P. Keenan, and D. J. Christian, Sci. 323, 1582 (2009).

⁹P. Song and V. M. Vasyliūnas, J. Geophys. Res.: Space Phys. **116** (A9), A09104, https://doi.org/10.1029/2011JA016679 (2011).